First-principles study on structural, dielectric, and dynamical properties for three BN polytypes

Nobuko Ohba, Kazutoshi Miwa, Naoyuki Nagasako, and Atsuo Fukumoto
Toyota Central Research & Development Laboratories, Inc., Nagakute, Aichi 480-1192, Japan
(Received 19 September 2000; published 1 March 2001)

We report the results of first-principles calculations on the structural properties (lattice constants and internal parameters), dielectric properties (macroscopic and static dielectric constants, and Born effective charge tensors), and dynamical properties (Γ-phonon frequencies) for the three polytypes of BN: the cubic zinc-blende structure (*c*-BN), the wurtzite structure (*w*-BN), and the hexagonal structure (*h*-BN). Our calculations were performed with the ultrasoft pseudopotential method and the linear response approach based on density-functional perturbation theory. By comparing the cohesive energies, we found that the *c*-BN structure is the most stable among the three polytypes at zero temperature. The computed equilibrium structural parameters, bulk moduli, and dielectric properties are in good agreement with the experimental data except for the lattice constant *c* of *h*-BN and the macroscopic dielectric constant along the *c* axis of *h*-BN. The Γ-phonon frequencies of *c*-BN and *w*-BN are close to each other. In order to distinguish *c*-BN and *w*-BN by Raman spectroscopy, it turns out that we should investigate the two Raman active E_2 modes that exist only in *w*-BN.

DOI: 10.1103/PhysRevB.63.115207 PACS number(s): 78.30.Fs, 63.20.−e, 77.22.−d

I. INTRODUCTION

In recent years, there have been many experiments and theoretical studies on the properties of boron nitride (BN). This is due to the fascinating properties of the cubic zinc-blende structure BN (*c*-BN), such as high bulk modulus, high thermal conductivity, high melting point, large band gap, and low dielectric constant. Because of these properties, *c*-BN is expected to be applicable for protective coating films and modern microelectronic devices at high temperature. It is known that there are three polytypes in BN. The cubic zinc-blende structure BN and the wurtzite structure BN (*w*-BN) resemble cubic and hexagonal diamond, respectively. The hexagonal structure of BN (*h*-BN) is similar to the structure of graphite. These structures are shown in Fig. 1.

It was suggested by previous experiment[1] that *h*-BN was the stable phase under ambient conditions, and *c*-BN and *w*-BN were synthesized from *h*-BN at high temperature and high pressure. However, recent experimental results[2,3] have pointed out that *c*-BN is the thermodynamically stable phase under ambient conditions and *h*-BN becomes stable at temperatures of about 900–1500 °C. Another phase, *w*-BN, is metastable above a pressure of 10 GPa.[4] Although *c*-BN is the stable phase under standard conditions, it is very difficult to produce single crystals by chemical or physical vapor deposition or high-pressure synthesis. Furthermore, several properties, such as the hardness, differ in the three polytypes of BN, and so quantification of the crystal structures has become much more important. However, there is a lack of data from infrared reflectivity (IR) or Raman spectroscopy experiments on BN, which would be useful for the quantitative analysis of crystal structures.

First-principles calculations based on density-functional theory in the local-density approximation (LDA) are widely performed in these days. These are computational techniques that predict the ground-state properties of materials with sufficient accuracy using no experimental values. The development of computational techniques such as ultrasoft pseudopotentials[5] has improved the reliability of the calculations for materials containing first-row elements in the periodic table or transition metals, which have localized electrons near the nucleus.

There have been several theoretical investigations of the ground-state properties of BN. However, there are disagreements among them as to the stable structure and the bulk modulus. Although the orthogonalized linear combination of atomic orbitals calculation by Xu and Ching[6] concludes that *h*-BN is more stable than *c*-BN, the other calculations performed using pseudopotentials and plane waves[7–9] agree in predicting that *c*-BN has a lower energy than *h*-BN by about 0.06 eV/atom. Concerning the bulk modulus, the calculated values for *c*-BN are consistent with each other, but for *h*-BN there are various values ranging from 28 GPa to 335 GPa.[6–9] In spite of the fact that the low dielectric constant is one of the fascinating properties of BN, there are few systematic calculations of the dielectric properties for the three BN polytypes. On the other hand, since the phonon frequencies at the Γ point are important fundamental properties observed by Raman or IR spectroscopy, several first-principles calculations have been performed. For example, there is a phonon-dispersion calculation using the *ab initio* force-constant approach for *c*-BN and *h*-BN,[7] and a calculation within the framework of the self-consistent density-functional perturbation theory[10,11] (DFPT) for the lattice dynamical properties

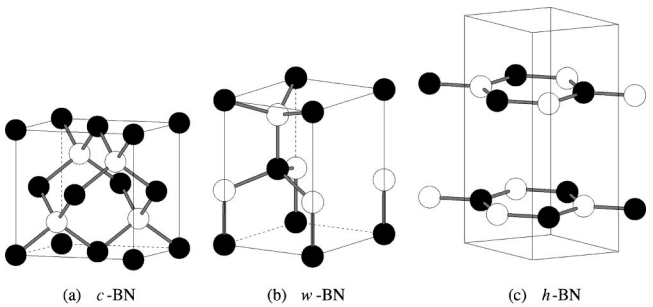

FIG. 1. The structures of the three BN polytypes. Black and white spheres denote B and N atoms, respectively.

of *c*-BN and *w*-BN.[12] However, as far as we know, no calculations comparing the Γ-phonon frequencies for the three polytypes of BN (*c*-BN, *w*-BN and *h*-BN) on the same footing have been reported yet.

In this paper, we report the results of first-principles calculations on the structural properties (lattice constants and internal parameters), dielectric properties (macroscopic and static dielectric constants and Born effective charge tensors), and Γ-phonon frequencies for the three polytypes of BN using the ultrasoft pseudopotential method and density-functional perturbation theory. In Sec. II, we describe the method of calculation. In Sec. III, we show the results for optimized structural parameters, dielectric properties, and dynamical properties at the Γ point, for the three polytypes of BN. We summarize this study in Sec. IV.

II. COMPUTATIONAL METHOD

A. Total energy calculations

We have performed a first-principles calculation of the three BN polytypes based on density-functional theory with the local-density approximation[13] and the ultrasoft pseudopotential technique.[5] The exchange-correlation interactions are described by the Perdew-Wang form.[14] In the pseudopotential generation scheme, the pseudo wave functions are constructed using the optimized potential method proposed by Rappe *et al.*[15] A similar scheme is applied to generate pseudo-charge-augmentation functions.

In solid-state calculations, the cutoff energy of the plane waves to expand the wave functions is set to be 20 hartrees. Although the cutoff energy for the charge densities is generally four times as large as that for wave functions in norm-conserving pseudopotential schemes, the ultrasoft pseudopotential calculations require a larger cutoff than in norm-conserving cases because of the presence of the augmentation charge. Therefore, it is chosen to be 100 hartrees in order to accurately expand the augmentation charge. We checked that these cutoff energies gave good convergence of total energy within 0.05 mhartrees/atom. Integrals over the Brillouin zone were approximated by sums on $(8\times8\times8)$, $(8\times8\times6)$, and $(10\times10\times4)$ Monkhorst-Pack **k**-point meshes[16] for *c*-BN, *w*-BN, and *h*-BN, respectively. The method for minimizing the Kohn-Sham energy functional is described in Ref. 17 and the Broyden charge density mixing technique[18] is employed in the present study.

B. Structural optimization

The equilibrium structural properties of *c*-BN are obtained by minimization of the total energy with respect to the unit cell volume. The total energies calculated at several lattice constants are fitted to Murnaghan's equation of state[19] in order to determine the equilibrium lattice constant and the bulk modulus. For *w*-BN, which has lower symmetry than *c*-BN, evaluation of the forces acting on atoms and the macroscopic stress tensor helps us to find the stable structure, because the atomic forces and the stress tensor must vanish in that structure. We have applied the Broyden algorithm to renew the structural parameters with the atomic forces and the stress tensor during the relaxation process. This process is continued until the remaining force and stress become less than 1×10^{-4} hartrees/bohr and 0.1 GPa, respectively. The bulk modulus of *w*-BN is obtained by fitting the energy-volume data to Murnaghan's equation of state. At this point, the energy-volume data are calculated by optimizing the lattice constants a,c and the internal parameter under a suitable external hydrostatic pressure in order to take account of the anisotropy of *w*-BN. The procedure to determine the equilibrium lattice constants and bulk modulus of *h*-BN is similar to that for *w*-BN. However, the relaxation process for *h*-BN can be carried out using only the stress tensor as an input, because the atomic forces vanish automatically due to the crystal symmetry.

In utilizing the macroscopic stress tensor for structural optimization, one should pay attention to the fact that, in general, the stress tensor derived from the total energy does not coincide with that computed analytically by a stress calculation. This discrepancy is called Pulay stress[20] by analogy with the Pulay force.[21] The Pulay stress is caused by the constant cutoff energy truncation for the plane-wave basis set, which causes a variation of the number of plane waves on varying the size of a unit cell. Although we have chosen a fairly large cutoff energy, the Pulay stress is not negligible. In order to remove the Pulay stress, the modification of the kinetic energy term proposed by Bernasconi *et al.*[22] is adopted during the relaxation process.

C. Linear response theory

The macroscopic dielectric constant is related to the second derivative of the total energy with respect to external electric field, and the dynamical matrix at the Γ point of the Brillouin zone is directly linked to the second derivative of the total energy with respect to the atomic displacements. The Born effective charge tensor is formulated as the mixed second derivative mentioned above. The calculations of such linear response functions have been made within the framework of the self-consistent density-functional perturbation theory.[10,11] The computational methods described in Refs. 10 and 11 are for the norm-conserving pseudopotential scheme. Dal Corso *et al.*[23] generalized DFPT for lattice dynamics in the ultrasoft pseudopotential scheme. We have extended it further for the response to an electric field.

According to Bloch's theorem, a wave function $\psi_{n\mathbf{k}}(\mathbf{r})$ can be decomposed into the product of a phase factor and a periodic function $u_{n\mathbf{k}}(\mathbf{r})$,

$$\psi_{n\mathbf{k}}(\mathbf{r})=\frac{1}{\sqrt{\Omega}}e^{i\mathbf{k}\cdot\mathbf{r}}u_{n\mathbf{k}}(\mathbf{r}), \tag{1}$$

where Ω is the volume of the unit cell, and n and $\mathbf{k}$ label the band and the wave vector of the wave function, respectively.

In the ultrasoft pseudopotential scheme, the second derivative of the total energy with respect to an electric field along direction $\alpha(\varepsilon_\alpha)$ and along direction $\beta(\varepsilon_\beta)$ is given by

$$\frac{\partial^2 E_{tot}}{\partial \varepsilon_\alpha \partial \varepsilon_\beta} = \frac{1}{(2\pi)^3}\int_{BZ} d\mathbf{k} \sum_n^{occ} s[\langle u_{n\mathbf{k}}^{\varepsilon_\alpha}| P_{c,\mathbf{k}}^* (H_{\mathbf{k},\mathbf{k}}^{(0)} - \varepsilon_{n\mathbf{k}}^{(0)} S_{\mathbf{k},\mathbf{k}}^{(0)}) P_{c,\mathbf{k}} |u_{n\mathbf{k}}^{\varepsilon_\beta}\rangle + \langle u_{n\mathbf{k}}^{\varepsilon_\beta}| P_{c,\mathbf{k}}^* (H_{\mathbf{k},\mathbf{k}}^{(0)} - \varepsilon_{n\mathbf{k}}^{(0)} S_{\mathbf{k},\mathbf{k}}^{(0)}) P_{c,\mathbf{k}} |u_{n\mathbf{k}}^{\varepsilon_\alpha}\rangle + \langle \varphi_{n\mathbf{k}}^{k_\beta}| P_{c,\mathbf{k}} |u_{n\mathbf{k}}^{\varepsilon_\beta}\rangle$$

$$+ \langle \varphi_{n\mathbf{k}}^{k_\beta}| P_{c,\mathbf{k}} |u_{n\mathbf{k}}^{\varepsilon_\alpha}\rangle + \langle u_{n\mathbf{k}}^{\varepsilon_\alpha}| P_{c,\mathbf{k}}^* |\varphi_{n\mathbf{k}}^{k_\beta}\rangle + \langle u_{n\mathbf{k}}^{\varepsilon_\beta}| P_{c,\mathbf{k}}^* |\varphi_{n\mathbf{k}}^{k_\alpha}\rangle] + \int\int \frac{\delta^2 E_{Hxc}}{\delta\rho(\mathbf{r}_1)\delta\rho(\mathbf{r}_2)}\Big|_{\rho^{(0)}} \rho^{\varepsilon_\alpha}(\mathbf{r}_1)\rho^{\varepsilon_\beta}(\mathbf{r}_2) d\mathbf{r}_1 d\mathbf{r}_2, \tag{2}$$

$$|\varphi_{n\mathbf{k}}^{k_\alpha}\rangle = S_{\mathbf{k},\mathbf{k}}^{(0)} P_{c,\mathbf{k}} |i u_{n\mathbf{k}}^{k_\alpha}\rangle + \sum_{Iij} [|p_{i\mathbf{k}}^{I(0)}\rangle Q_{ij}^I \langle p_{j\mathbf{k}}^{Ik_\alpha}| i u_{n\mathbf{k}}^{(0)}\rangle + |p_{i\mathbf{k}}^{I(0)}\rangle d_{ij,\alpha}^I \langle p_{j\mathbf{k}}^{I(0)}| u_{n\mathbf{k}}^{(0)}\rangle], \tag{3}$$

$$Q_{ij}^I = \int \tilde{q}_{ij}^I(\mathbf{r}) d\mathbf{r}, \tag{4}$$

$$d_{ij,\alpha}^I = \int r_\alpha \tilde{q}_{ij}^I(\mathbf{r}) d\mathbf{r}, \tag{5}$$

with the first derivative of the charge density with respect to ε_α

$$\rho^{\varepsilon_\alpha}(\mathbf{r}) = \frac{1}{(2\pi)^3}\int_{BZ} d\mathbf{k} \sum_n^{occ} s[u_{n\mathbf{k}}^{\varepsilon_\alpha *}(\mathbf{r}) P_{c,\mathbf{k}}^* K_{\mathbf{k},\mathbf{k}}^{(0)}(\mathbf{r}) u_{n\mathbf{k}}^{(0)}(\mathbf{r}) + u_{n\mathbf{k}}^{(0)*}(\mathbf{r}) K_{\mathbf{k},\mathbf{k}}^{(0)}(\mathbf{r}) P_{c,\mathbf{k}} u_{n\mathbf{k}}^{\varepsilon_\alpha}(\mathbf{r})], \tag{6}$$

$$K(\mathbf{r}) = |\mathbf{r}\rangle\langle\mathbf{r}| + \sum_{Iij} |p_i^I\rangle \tilde{q}_{ij}^I(\mathbf{r}) \langle p_j^I|, \tag{7}$$

where the integration is performed over the whole Brillouin zone, the summation runs over the occupied states n, s is the spin degeneracy, $u_{n\mathbf{k}}^{\varepsilon_\alpha}$ is a shorthand notation for the first derivative of $u_{n\mathbf{k}}$ with respect to the electric field ε_α, $P_{c,\mathbf{k}} = 1 - \Sigma_n^{occ} |u_{n\mathbf{k}}^{(0)}\rangle\langle u_{n\mathbf{k}}^{(0)}| S_{\mathbf{k},\mathbf{k}}^{(0)}$ is the projector upon the conduction bands, $P_{c,\mathbf{k}}^*$ indicates the Hermitian conjugate of $P_{c,\mathbf{k}}$, the superscript (0) means the unperturbed state, and $H^{(0)}$, $\varepsilon_{n\mathbf{k}}^{(0)}$, and $S^{(0)}$ correspond to the unperturbed Hamiltonian, the eigenvalues of $H^{(0)}$, and the overlap matrix, respectively. E_{Hxc} is the Hartree and exchange-correlation energy functional of the charge density $\rho(\mathbf{r})$. We have defined for a generic operator O that $O_{\mathbf{k},\mathbf{k}'} = e^{-i\mathbf{k}\cdot\mathbf{r}} O e^{i\mathbf{k}'\cdot\mathbf{r}'}$. The term $|\varphi_{n\mathbf{k}}^{k_\alpha}\rangle$ which includes the first derivative of the wave function with respect to the wave vector originates in treating the electric field as the longitudinal one.[10] The projectors p_i^I and the charge augmentation functions $\tilde{q}_{ij}^I(\mathbf{r})$, for an atom of species I, are the basic ingredients of the ultrasoft pseudopotential scheme. Here $\{i,j\}$ is a composite index labeling the angular momentum (lm) and radial indices of the projectors.

From Eq. (2) and the generalized orthogonal constraint $\langle u_{n\mathbf{k}}^{\varepsilon_\alpha}| S_{\mathbf{k},\mathbf{k}}^{(0)} |u_{n\mathbf{k}}^{(0)}\rangle + \langle u_{n\mathbf{k}}^{(0)}| S_{\mathbf{k},\mathbf{k}}^{(0)} |u_{n\mathbf{k}}^{\varepsilon_\alpha}\rangle = 0$, we deduce the following Sternheimer equation:

$$P_{c,\mathbf{k}}^* (H_{\mathbf{k},\mathbf{k}}^{(0)} - \varepsilon_{n\mathbf{k}}^{(0)} S_{\mathbf{k},\mathbf{k}}^{(0)}) P_{c,\mathbf{k}} |u_{n\mathbf{k}}^{\varepsilon_\alpha}\rangle + P_{c,\mathbf{k}}^* |\vartheta_{n\mathbf{k}}^{k_\alpha}\rangle = 0, \tag{8}$$

with

$$|\vartheta_{n\mathbf{k}}^{k_\alpha}\rangle = |\varphi_{n\mathbf{k}}^{k_\alpha}\rangle + \sum_{Iij} |p_{i\mathbf{k}}^{I(0)}\rangle \int w_{Hxc}^{\varepsilon_\alpha}(\mathbf{r}) \tilde{q}_{ij}^{I(0)}(\mathbf{r}) d\mathbf{r} \times \langle p_{j\mathbf{k}}^{I(0)}| u_{n\mathbf{k}}^{(0)}\rangle, \tag{9}$$

$$w_{Hxc}^{\varepsilon_\alpha}(\mathbf{r}) = \int \frac{\delta^2 E_{Hxc}}{\delta\rho(\mathbf{r})\delta\rho(\mathbf{r}')}\Big|_{\rho^{(0)}} \rho^{\varepsilon_\alpha}(\mathbf{r}') d\mathbf{r}'. \tag{10}$$

The Sternheimer Eq. (8) is solved self-consistently because the perturbed term $w_{Hxc}^{\varepsilon_\alpha}(\mathbf{r})$ depends on the derivative of the charge density $\rho^{\varepsilon_\alpha}$, and as Eq. (6) shows $\rho^{\varepsilon_\alpha}$ is a functional of $P_{c,\mathbf{k}}|u_{n\mathbf{k}}^{\varepsilon_\alpha}\rangle$. The conjugate-gradient algorithm is employed to solve the Sternheimer equation and the mixing for updating the first derivative of the charge density is performed with the Broyden charge mixing technique.

The first derivative of the wave function with respect to the wave vector can be determined by the following Sternheimer equation:

$$P_{c,\mathbf{k}}^* (H_{\mathbf{k},\mathbf{k}}^{(0)} - \varepsilon_{n\mathbf{k}}^{(0)} S_{\mathbf{k},\mathbf{k}}^{(0)}) P_{c,\mathbf{k}} |u_{n\mathbf{k}}^{k_\alpha}\rangle + P_{c,\mathbf{k}}^* (H_{\mathbf{k},\mathbf{k}}^{k_\alpha} - \varepsilon_{n\mathbf{k}}^{(0)} S_{\mathbf{k},\mathbf{k}}^{k_\alpha}) |u_{n\mathbf{k}}^{(0)}\rangle = 0, \tag{11}$$

with

$$H_{\mathbf{k},\mathbf{k}}^{k_\alpha} = T_{\mathbf{k},\mathbf{k}}^{k_\alpha} + v_{NL,\mathbf{k},\mathbf{k}}^{k_\alpha} + \sum_{Iij} \Big[|p_{i\mathbf{k}}^{Ik_\alpha}\rangle \int V_{eff}^{(0)}(\mathbf{r}) \tilde{q}_{ij}^{I(0)}(\mathbf{r}) d\mathbf{r} \times \langle p_{j\mathbf{k}}^{I(0)}| + |p_{i\mathbf{k}}^{I(0)}\rangle \int V_{eff}^{(0)}(\mathbf{r}) \tilde{q}_{ij}^{I(0)}(\mathbf{r}) d\mathbf{r} \langle p_{j\mathbf{k}}^{Ik_\alpha}| \Big], \tag{12}$$

$$V_{eff}^{(0)}(\mathbf{r}) = v_L^{(0)}(\mathbf{r}) + v_{Hxc}^{(0)}(\mathbf{r}), \tag{13}$$

where $T_{\mathbf{k},\mathbf{k}}^{k_\alpha}$, $v_{NL,\mathbf{k},\mathbf{k}}^{k_\alpha}$, and $p_{i\mathbf{k}}^{Ik_\alpha}$ are the first derivative of the kinetic energy operator, the nonlocal part of the pseudopotential and the projector with respect to the wave vector k_α, respectively. V_{eff} denotes the sum of the local part of the pseudopotential v_L and the Hartree and exchange-correlation

potential v_{Hxc}. Since Eq. (11) does not include the term ρ^{k_α}, $P_{c,\mathbf{k}}|u_{n\mathbf{k}}^{k_\alpha}\rangle$ can be computed directly.

The dynamical matrix at the Γ point is separated into the Ewald part and the electronic part. The Ewald part can be found in Ref. 11. The electronic part is expressed by the second derivative of the electronic contribution to the total energy with respect to the atomic displacements as follows:

$$\begin{aligned}\frac{\partial^2 E_{el}}{\partial R_{I\alpha}\partial R_{J\beta}}=&\frac{1}{(2\pi)^3}\int_{BZ}d\mathbf{k}\Bigg\{\sum_n^{occ} s[\langle u_{n\mathbf{k}}^{R_{I\alpha}}|P_{c,\mathbf{k}}^*(H_{\mathbf{k},\mathbf{k}}^{(0)}-\varepsilon_{n\mathbf{k}}^{(0)}S_{\mathbf{k},\mathbf{k}}^{(0)})P_{c,\mathbf{k}}|u_{n\mathbf{k}}^{R_{J\beta}}\rangle+\langle u_{n\mathbf{k}}^{R_{J\beta}}|P_{c,\mathbf{k}}^*(H_{\mathbf{k},\mathbf{k}}^{(0)}-\varepsilon_{n\mathbf{k}}^{(0)}S_{\mathbf{k},\mathbf{k}}^{(0)})P_{c,\mathbf{k}}|u_{n\mathbf{k}}^{R_{I\alpha}}\rangle\\&+\langle u_{n\mathbf{k}}^{(0)}|(H'^{R_{I\alpha}}_{\mathbf{k},\mathbf{k}}-\varepsilon_{n\mathbf{k}}^{(0)}S_{\mathbf{k},\mathbf{k}}^{R_{I\alpha}})P_{c,\mathbf{k}}|u_{n\mathbf{k}}^{R_{J\beta}}\rangle+\langle u_{n\mathbf{k}}^{(0)}|(H'^{R_{J\beta}}_{\mathbf{k},\mathbf{k}}-\varepsilon_{n\mathbf{k}}^{(0)}S_{\mathbf{k},\mathbf{k}}^{R_{J\beta}})P_{c,\mathbf{k}}|u_{n\mathbf{k}}^{R_{I\alpha}}\rangle+\langle u_{n\mathbf{k}}^{R_{I\alpha}}|P_{c,\mathbf{k}}^*(H'^{R_{J\beta}}_{\mathbf{k},\mathbf{k}}-\varepsilon_{n\mathbf{k}}^{(0)}S_{\mathbf{k},\mathbf{k}}^{R_{J\beta}})|u_{n\mathbf{k}}^{(0)}\rangle\\&+\langle u_{n\mathbf{k}}^{R_{J\beta}}|P_{c,\mathbf{k}}^*(H'^{R_{I\alpha}}_{\mathbf{k},\mathbf{k}}-\varepsilon_{n\mathbf{k}}^{(0)}S_{\mathbf{k},\mathbf{k}}^{R_{I\alpha}})|u_{n\mathbf{k}}^{(0)}\rangle+\langle u_{n\mathbf{k}}^{(0)}|(H'^{R_{I\alpha}R_{J\beta}}_{\mathbf{k},\mathbf{k}}-\varepsilon_{n\mathbf{k}}^{(0)}S_{\mathbf{k},\mathbf{k}}^{R_{I\alpha}R_{J\beta}})|u_{n\mathbf{k}}^{(0)}\rangle]-\sum_{mn}^{occ} s\langle u_{n\mathbf{k}}^{(0)}|S_{\mathbf{k},\mathbf{k}}^{R_{I\alpha}}|u_{m\mathbf{k}}^{(0)}\rangle\langle u_{m\mathbf{k}}^{(0)}|H'^{R_{J\beta}}_{\mathbf{k},\mathbf{k}}\\&-\varepsilon_{n\mathbf{k}}^{(0)}S_{\mathbf{k},\mathbf{k}}^{R_{J\beta}}|u_{n\mathbf{k}}^{(0)}\rangle-\sum_{mn}^{occ} s\langle u_{n\mathbf{k}}^{(0)}|S_{\mathbf{k},\mathbf{k}}^{R_{J\beta}}|u_{m\mathbf{k}}^{(0)}\rangle\langle u_{m\mathbf{k}}^{(0)}|H'^{R_{I\alpha}}_{\mathbf{k},\mathbf{k}}-\varepsilon_{n\mathbf{k}}^{(0)}S_{\mathbf{k},\mathbf{k}}^{R_{I\alpha}}|u_{n\mathbf{k}}^{(0)}\rangle\Bigg\}\\&+\int\int\frac{\delta^2 E_{Hxc}}{\delta\rho(\mathbf{r}_1)\delta\rho(\mathbf{r}_2)}\Bigg|_{\rho^{(0)}}\rho^{R_{I\alpha}}(\mathbf{r}_1)\rho^{R_{J\beta}}(\mathbf{r}_2)d\mathbf{r}_1 d\mathbf{r}_2+\frac{d^2E_{xc}}{dR_{I\alpha}dR_{J\beta}}\Bigg|_{\rho^{(0)}},\end{aligned}\tag{14}$$

$$\begin{aligned}\rho^{R_{I\alpha}}(\mathbf{r})=&\frac{1}{(2\pi)^3}\int_{BZ}d\mathbf{k}\Bigg\{\sum_n^{occ} s[u_{n\mathbf{k}}^{(0)*}(\mathbf{r})K_{\mathbf{k},\mathbf{k}}^{(0)}(\mathbf{r})P_{c,\mathbf{k}}u_{n\mathbf{k}}^{R_{I\alpha}}(\mathbf{r})+u_{n\mathbf{k}}^{R_{I\alpha}*}(\mathbf{r})P_{c,\mathbf{k}}^*K_{\mathbf{k},\mathbf{k}}^{(0)}(\mathbf{r})u_{n\mathbf{k}}^{(0)}(\mathbf{r})+u_{n\mathbf{k}}^{(0)*}(\mathbf{r})K_{\mathbf{k},\mathbf{k}}^{R_{I\alpha}}(\mathbf{r})u_{n\mathbf{k}}^{(0)}(\mathbf{r})]\\&-\sum_{mn}^{occ} s\langle u_{n\mathbf{k}}^{(0)}|S^{R_{I\alpha}}|u_{m\mathbf{k}}^{(0)}\rangle u_{m\mathbf{k}}^{(0)*}(\mathbf{r})K_{\mathbf{k},\mathbf{k}}^{(0)}(\mathbf{r})u_{n\mathbf{k}}^{(0)}(\mathbf{r})\Bigg\},\end{aligned}\tag{15}$$

$$H'^{R_{I\alpha}}_{\mathbf{k},\mathbf{k}}=v_{NL,\mathbf{k},\mathbf{k}}^{R_{I\alpha}}+V_{eff}^{(0)}K_{\mathbf{k},\mathbf{k}}^{R_{I\alpha}}+V'^{R_{I\alpha}}_{eff}K_{\mathbf{k},\mathbf{k}}^{(0)},\tag{16}$$

$$H'^{R_{I\alpha}R_{J\beta}}_{\mathbf{k},\mathbf{k}}=v_{NL,\mathbf{k},\mathbf{k}}^{R_{I\alpha}R_{J\beta}}+V_{eff}^{(0)}K_{\mathbf{k},\mathbf{k}}^{R_{I\alpha}R_{J\beta}}+V'^{R_{I\alpha}}_{eff}K_{\mathbf{k},\mathbf{k}}^{R_{J\beta}}+V'^{R_{J\beta}}_{eff}K_{\mathbf{k},\mathbf{k}}^{R_{I\alpha}}+v_L^{R_{I\alpha}R_{J\beta}}K_{\mathbf{k},\mathbf{k}}^{(0)},\tag{17}$$

$$V'^{R_{I\alpha}}_{eff}(\mathbf{r})=v_L^{R_{I\alpha}}(\mathbf{r})+v_{Hxc}^{R_{I\alpha}}(\mathbf{r}),\tag{18}$$

$$VK=V(\mathbf{r})+\sum_{Iij}|p_i^I\rangle\int V(\mathbf{r}')\tilde{q}_{ij}^{I(0)}(\mathbf{r}')d\mathbf{r}'\langle p_j^I|,\tag{19}$$

where $R_{I\alpha}$ denotes the atomic displacement of atom I along direction α and $X^{R_{I\alpha}R_{J\beta}}$ is the shorthand notation for the second derivative of X with respect to $R_{I\alpha}$ and $R_{J\beta}$. $(d^2E_{xc}/dR_{I\alpha}dR_{J\beta})|_{\rho^{(0)}}$ is the second derivative of the exchange-correlation functional, which appears when the partial core correction[24] is taken into account.

The Sternheimer equation for the derivative of the wave function with respect to the atomic displacements is

$$P_{c,\mathbf{k}}^*(H_{\mathbf{k},\mathbf{k}}^{(0)}-\varepsilon_{n\mathbf{k}}^{(0)}S_{\mathbf{k},\mathbf{k}}^{(0)})P_{c,\mathbf{k}}|u_{n\mathbf{k}}^{R_{I\alpha}}\rangle+P_{c,\mathbf{k}}^*(H_{\mathbf{k},\mathbf{k}}^{R_{I\alpha}}-\varepsilon_{n\mathbf{k}}^{(0)}S_{\mathbf{k},\mathbf{k}}^{R_{I\alpha}})|u_{n\mathbf{k}}^{(0)}\rangle=0,\tag{20}$$

with

$$H_{\mathbf{k},\mathbf{k}}^{R_{I\alpha}}=v_{NL,\mathbf{k},\mathbf{k}}^{R_{I\alpha}}+V_{eff}^{(0)}K_{\mathbf{k},\mathbf{k}}^{R_{I\alpha}}+V_{eff}^{R_{I\alpha}}K_{\mathbf{k},\mathbf{k}}^{(0)},\tag{21}$$

$$V_{eff}^{R_{I\alpha}}(\mathbf{r})=V'^{R_{I\alpha}}_{eff}(\mathbf{r})+\int\frac{\delta^2E_{Hxc}}{\delta\rho(\mathbf{r})\delta\rho(\mathbf{r}')}\Bigg|_{\rho^{(0)}}\rho^{R_{I\alpha}}(\mathbf{r}')d\mathbf{r}'.\tag{22}$$

Finally, the mixed second derivative of the total energy with respect to $R_{I\alpha}$ and ε_β, which is required for the Born effective charge tensor, is

$$\frac{\partial^2 E_{tot}}{\partial R_{I\alpha}\partial\varepsilon_\beta}=\frac{1}{(2\pi)^3}\int_{BZ}d\mathbf{k}\Bigg\{\sum_n^{occ} s\Bigg[\langle u_{n\mathbf{k}}^{R_{I\alpha}}|P_{c,\mathbf{k}}^*(H_{\mathbf{k},\mathbf{k}}^{(0)}-\varepsilon_{n\mathbf{k}}^{(0)}S_{\mathbf{k},\mathbf{k}}^{(0)})P_{c,\mathbf{k}}|u_{n\mathbf{k}}^{\varepsilon_\beta}\rangle+\langle u_{n\mathbf{k}}^{\varepsilon_\beta}|P_{c,\mathbf{k}}^*(H_{\mathbf{k},\mathbf{k}}^{(0)}-\varepsilon_{n\mathbf{k}}^{(0)}S_{\mathbf{k},\mathbf{k}}^{(0)})P_{c,\mathbf{k}}|u_{n\mathbf{k}}^{R_{I\alpha}}\rangle+\langle u_{n\mathbf{k}}^{(0)}|(H'^{R_{I\alpha}}_{\mathbf{k},\mathbf{k}}$$
$$-\varepsilon_{n\mathbf{k}}^{(0)}S_{\mathbf{k},\mathbf{k}}^{R_{I\alpha}})P_{c,\mathbf{k}}|u_{n\mathbf{k}}^{\varepsilon_\beta}\rangle+\langle u_{n\mathbf{k}}^{\varepsilon_\beta}|P_{c,\mathbf{k}}^*(H'^{R_{I\alpha}}_{\mathbf{k},\mathbf{k}}-\varepsilon_{n\mathbf{k}}^{(0)}S_{\mathbf{k},\mathbf{k}}^{R_{I\alpha}})|u_{n\mathbf{k}}^{(0)}\rangle+\langle\varphi_{n\mathbf{k}}^{k_\beta}|P_{c,\mathbf{k}}|u_{n\mathbf{k}}^{R_{I\alpha}}\rangle+\langle u_{n\mathbf{k}}^{R_{I\alpha}}|P_{c,\mathbf{k}}^*|\varphi_{n\mathbf{k}}^{k_\beta}\rangle+\langle\varphi_{n\mathbf{k}}^{R_{I\alpha},k_\beta}|u_{n\mathbf{k}}^{(0)}\rangle$$
$$+\langle u_{n\mathbf{k}}^{(0)}|\varphi_{n\mathbf{k}}^{R_{I\alpha},k_\beta}\rangle+\delta_{\alpha\beta}\sum_{Iij}\langle u_{n\mathbf{k}}^{(0)}|p_{i,\mathbf{k}}^{I(0)}\rangle Q_{ij}^I\langle p_{j,\mathbf{k}}^{I(0)}|u_{n\mathbf{k}}^{(0)}\rangle\Bigg]-\sum_{mn}^{occ} s\Bigg[\sum_{Iij}(\langle u_{n\mathbf{k}}^{(0)}|p_{i\mathbf{k}}^{IR_{I\alpha}}\rangle Q_{ij}^I\langle p_{j\mathbf{k}}^{I(0)}|u_{m\mathbf{k}}^{(0)}\rangle)\langle u_{m\mathbf{k}}^{(0)}|\varphi_{n\mathbf{k}}^{k_\beta}\rangle$$
$$+\langle\varphi_{n\mathbf{k}}^{k_\beta}|u_{m\mathbf{k}}^{(0)}\rangle\sum_{Iij}(\langle u_{m\mathbf{k}}^{(0)}|p_{i\mathbf{k}}^{I(0)}\rangle Q_{ij}^I\langle p_{j\mathbf{k}}^{IR_{I\alpha}}|u_{n\mathbf{k}}^{(0)}\rangle)\Bigg]\Bigg\}+\int\int\left.\frac{\delta^2E_{Hxc}}{\delta\rho(\mathbf{r}_1)\delta\rho(\mathbf{r}_2)}\right|_{\rho^{(0)}}\rho^{R_{I\alpha}}(\mathbf{r}_1)\rho^{\varepsilon_\beta}(\mathbf{r}_2)d\mathbf{r}_1d\mathbf{r}_2, \tag{23}$$

$$|\varphi_{n\mathbf{k}}^{R_{I\alpha},k_\beta}\rangle=\sum_{Iij}[|p_{i\mathbf{k}}^{IR_{I\alpha}}\rangle Q_{ij}^I\langle p_{j\mathbf{k}}^{I(0)}|P_{c,\mathbf{k}}|iu_{n\mathbf{k}}^{k_\beta}\rangle+|p_{i\mathbf{k}}^{IR_{I\alpha}}\rangle Q_{ij}^I\langle p_{j\mathbf{k}}^{Ik_\beta}|iu_{n\mathbf{k}}^{(0)}\rangle+|p_{i\mathbf{k}}^{IR_{I\alpha}}\rangle d_{ij,\beta}^I\langle p_{j\mathbf{k}}^{I(0)}|u_{n\mathbf{k}}^{(0)}\rangle]. \tag{24}$$

In this stationary expression [Eq. (23)], the first derivative of the wave functions with respect to atomic displacements, the electric field, and the wave vector are required. In the nonstationary expression descrived below, the first derivative with respect to atomic displacements is unnecessary:

$$\frac{\partial^2 E_{tot}}{\partial R_{I\alpha}\partial\varepsilon_\beta}=\frac{1}{(2\pi)^3}\int_{BZ}d\mathbf{k}\Bigg\{\sum_n^{occ} s\Bigg[\langle u_{n\mathbf{k}}^{(0)}|(H'^{R_{I\alpha}}_{\mathbf{k},\mathbf{k}}-\varepsilon_{n\mathbf{k}}^{(0)}S_{\mathbf{k},\mathbf{k}}^{R_{I\alpha}})P_{c,\mathbf{k}}|u_{n\mathbf{k}}^{\varepsilon_\beta}\rangle+\langle u_{n\mathbf{k}}^{\varepsilon_\beta}|P_{c,\mathbf{k}}^*(H'^{R_{I\alpha}}_{\mathbf{k},\mathbf{k}}-\varepsilon_{n\mathbf{k}}^{(0)}S_{\mathbf{k},\mathbf{k}}^{R_{I\alpha}})|u_{n\mathbf{k}}^{(0)}\rangle+\langle\vartheta_{n\mathbf{k}}^{R_{I\alpha},k_\beta}|u_{n\mathbf{k}}^{(0)}\rangle$$
$$+\langle u_{n\mathbf{k}}^{(0)}|\vartheta_{n\mathbf{k}}^{R_{I\alpha},k_\beta}\rangle+\delta_{\alpha\beta}\sum_{Iij}\langle u_{n\mathbf{k}}^{(0)}|p_{i\mathbf{k}}^{I(0)}\rangle Q_{ij}^I\langle p_{j\mathbf{k}}^{I(0)}|u_{n\mathbf{k}}^{(0)}\rangle\Bigg]-\sum_{mn}^{occ} s\Bigg[\sum_{Iij}(\langle u_{n\mathbf{k}}^{(0)}|p_{i\mathbf{k}}^{IR_{I\alpha}}\rangle Q_{ij}^I\langle p_{j\mathbf{k}}^{I(0)}|u_{m\mathbf{k}}^{(0)}\rangle)\langle u_{m\mathbf{k}}^{(0)}|\vartheta_{n\mathbf{k}}^{k_\beta}\rangle$$
$$+\langle\vartheta_{n\mathbf{k}}^{k_\beta}|u_{m\mathbf{k}}^{(0)}\rangle\sum_{Iij}(\langle u_{m\mathbf{k}}^{(0)}|p_{i\mathbf{k}}^{I(0)}\rangle Q_{ij}^I\langle p_{j\mathbf{k}}^{IR_{I\alpha}}|u_{n\mathbf{k}}^{(0)}\rangle)\Bigg]\Bigg\}, \tag{25}$$

$$|\vartheta_{n\mathbf{k}}^{R_{I\alpha},k_\beta}\rangle=|\varphi_{n\mathbf{k}}^{R_{I\alpha},k_\beta}\rangle+\sum_{Iij}|p_{i\mathbf{k}}^{IR_{I\alpha}}\rangle\int w_{Hxc}^{\varepsilon_\beta}(\mathbf{r})\tilde{q}_{ij}^{I(0)}(\mathbf{r})d\mathbf{r}\langle p_{j\mathbf{k}}^{I(0)}|u_{n\mathbf{k}}^{(0)}\rangle. \tag{26}$$

Another nonstationary form is also possible, in which the first derivative with respect to the wave vector and the atomic displacements are needed:

$$\frac{\partial^2 E_{tot}}{\partial R_{I\alpha}\partial\varepsilon_\beta}=\frac{1}{(2\pi)^3}\int_{BZ}d\mathbf{k}\Bigg\{\sum_n^{occ} s\Bigg[\langle\varphi_{n\mathbf{k}}^{k_\beta}|P_{c,\mathbf{k}}|u_{n\mathbf{k}}^{R_{I\alpha}}\rangle+\langle u_{n\mathbf{k}}^{R_{I\alpha}}|P_{c,\mathbf{k}}^*|\varphi_{n\mathbf{k}}^{k_\beta}\rangle+\langle\varphi_{n\mathbf{k}}^{R_{I\alpha},k_\beta}|u_{n\mathbf{k}}^{(0)}\rangle+\langle u_{n\mathbf{k}}^{(0)}|\varphi_{n\mathbf{k}}^{R_{I\alpha},k_\beta}\rangle$$
$$+\delta_{\alpha\beta}\sum_{Iij}\langle u_{n\mathbf{k}}^{(0)}|p_i^{I(0)}\rangle Q_{ij}^I\langle p_j^{I(0)}|u_{n\mathbf{k}}^{(0)}\rangle\Bigg]-\sum_{mn}^{occ} s\Bigg[\sum_{Iij}(\langle u_{n\mathbf{k}}^{(0)}|p_{i\mathbf{k}}^{IR_{I\alpha}}\rangle Q_{ij}^I\langle p_{j\mathbf{k}}^{I(0)}|u_{m\mathbf{k}}^{(0)}\rangle)\langle u_{m\mathbf{k}}^{(0)}|\varphi_{n\mathbf{k}}^{k_\beta}\rangle$$
$$+\langle\varphi_{n\mathbf{k}}^{k_\beta}|u_{m\mathbf{k}}^{(0)}\rangle\sum_{Iij}(\langle u_{m\mathbf{k}}^{(0)}|p_{i\mathbf{k}}^{I(0)}\rangle Q_{ij}^I\langle p_{j\mathbf{k}}^{IR_{I\alpha}}|u_{n\mathbf{k}}^{(0)}\rangle)\Bigg]\Bigg\}. \tag{27}$$

We have used Eq. (25) for calculation of the Born effective charge tensors.

III. RESULTS

A. Structural properties

The optimized structural properties (lattice constants, internal parameters, bulk modulus, and cohesive energy) for the three polytypes of BN are shown in Table I. The cohesive energy is computed by subtracting the sum of the total energy of the isolated atoms including the spin-polarization energy from that of the solid.

As is well known, the lattice constants obtained by the LDA are a little smaller than the experimental values. But the error is less than 1% except for the lattice constant c of h-BN, and so it can be said that the calculated lattice constants and the experimental values are in good agreement. Previous calculations predicted the lattice constant c of h-BN in the range 6.439–6.66 Å.[6–9] The relatively large error in c of h-BN is due to its layer structure. The lattice constant c of h-BN is affected by a weak van der Waals interaction, while the lattice constant a is determined by the extremely short and strong ionic-covalent sp^2 bonding. Therefore, the variation of the cohesive energy with the relative length of c is much smaller than that with a, as shown in Figs. 2 and 3.

TABLE I. Calculated and experimental structural properties for the three polytypes of BN: lattice constants a,c (Å), internal parameter u, bulk modulus B (GPa), and cohesive energy E (hartrees/atom).

a	c	u	B	E	
		c-BN			
3.592			395	−0.2940	present
3.615					exp.[a]
3.615			370		calc.[b]
3.581			398	−0.2997	calc.[c]
3.593			395	−0.2379	calc.[d]
3.576			397	−0.2997	calc.[e]
3.591			397		calc.[f]
		w-BN			
2.532	4.188	0.3744	396	−0.2934	present
2.553	4.228				exp.[g]
2.536	4.199		390		calc.[b]
2.532	4.188	0.374	394	−0.2375	calc.[d]
2.521	4.165		401	−0.2990	calc.[e]
2.531	4.194	0.3751	399		calc.[f]
		h-BN			
2.496	6.498		26	−0.2919	present
2.504(2)	6.660(8)		36.7		exp.[h]
2.494	6.66		335		calc.[b]
2.489	6.481		28	−0.2975	calc.[c]
2.496	6.490		30.1	−0.2358	calc.[d]
2.486	6.439		261	−0.2977	calc.[e]

[a]Reference 25.
[b]Reference 6.
[c]Reference 7.
[d]Reference 8.
[e]Reference 9.
[f]Reference 12.
[g]Reference 26.
[h]Reference 27.

When c is lengthened (shortened) by 5% from the equilibrium value $c_0=6.4976$ Å, the change of the cohesive energy is only 0.05 (0.09) mhartrees/atom. On the other hand, as Fig. 3 shows, the variation of the stress is monotonic and large enough to allow estimation of the equilibrium lattice constant. Since the macroscopic stress tensor is employed to find the stable structure, we expect that the accuracy of the lattice constant c obtained by the present calculation is better than that obtained from the total energy variation. The discrepancy with the experimental data in c of h-BN may be remedied by using the generalized gradient approximation[28] for the exchange-correlation functional.

In the present study, the calculated bulk modulus of c-BN is 395 GPa and that of w-BN is 396 GPa. These values are close to that of diamond, 442 GPa.[29] Since the bulk modulus of h-BN is 26 GPa, it is not as hard as c-BN and w-BN. Theoretical values for the bulk modulus of h-BN vary from 28 to 335 GPa.[6–9] The reason is considered to be that the interaction along the c axis direction is so weak. The energy-volume data generated from isotropically compressed or expanded unit cells yield erroneous results for the bulk modulus, especially if the structures are strongly anisotropic. When we use the energy-volume data of isotropic compression and expansion, the calculated bulk modulus of h-BN is 253 GPa. This value differs greatly from the experimental value of 36.7 GPa obtained by Solozhenko *et al.*[27] We have checked the computational accuracy using the following relation between the bulk modulus B and the elastic constants C_{ij} of h-BN:

$$B=\frac{C_{33}(C_{11}+C_{12})-2(C_{13})^2}{C_{11}+C_{12}+2C_{33}-4C_{13}}. \tag{28}$$

The elastic constants of h-BN, C_{11},C_{12},C_{13}, and C_{33}, are shown in Table II, calculated from the elements of the stress tensor by applying several strains corresponding to $\pm 1\%$ of the equilibrium lattice constants. The bulk modulus obtained from Eq. (28) is 27 GPa. This is in reasonable agreement with the value of 26 GPa computed by total energy fitting.

By comparing the cohesive energy of the three BN polytypes, we predict that the c-BN structure is the most stable at zero temperature. The difference in cohesive energy between c-BN and w-BN is 0.6 mhartrees/atom, and that between

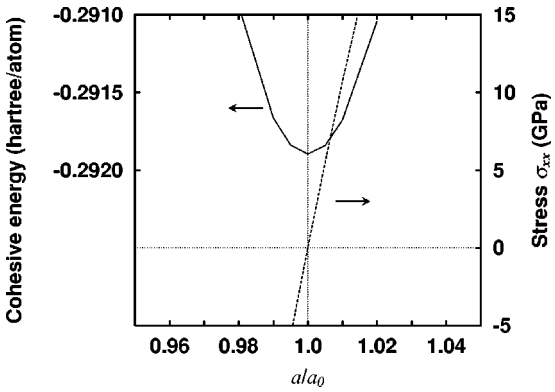

FIG. 2. Cohesive energy (solid line) and the macroscopic stress tensor element perpendicular to the c axis σ_{xx} (dashed line) vs relative length of a for h-BN. a_0 is the equilibrium lattice constant: $a_0=2.4959$ Å.

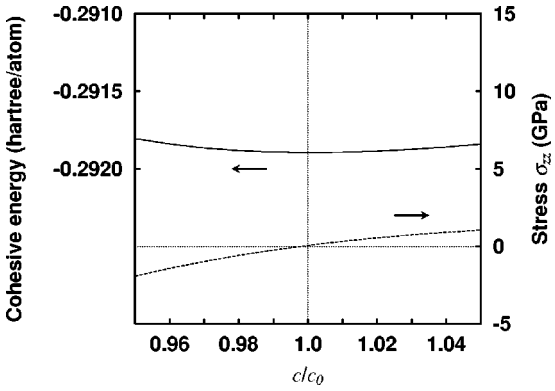

FIG. 3. Cohesive energy (solid line) and the macroscopic stress tensor element parallel to the c axis σ_{zz} (dashed line) vs relative length of c for h-BN. c_0 is the equilibrium lattice constant: $c_0=6.4976$ Å.

TABLE II. Calculated elastic constants (in GPa) of *h*-BN.

C_{11}	C_{12}	C_{13}	C_{33}
951.5	169.2	2.5	28.2

c-BN and *h*-BN is 2.1 mhartrees/atom. These results agree with other calculations using plane waves and pseudopotentials.[7–9,12]

B. Dielectric properties

The macroscopic dielectric constant ε_∞ is observed as a response to a uniform electric field, and the Born effective charge tensor Z^* is defined as the proportionality coefficient relating the macroscopic polarization and the displacement of atoms from their equilibrium positions. Knowledge of the macroscopic dielectric constant and the Born effective charge tensor is essential for describing the long-range dipolar contribution to the lattice dynamics of a polar crystal. The static dielectric constant ε_0 is calculated by adding the effects of the dipole interactions represented by the following two contributions to the macroscopic dielectric constant.[11] One is the Born effective charge tensor, and the other is the set of eigenvalues and eigenvectors of the dynamical matrix that determines the frequencies of the transverse optical (TO) mode. These calculated values for the three BN polytypes are shown in Table III. Here the Born effective charge tensors are given as absolute values and the acoustic sum rule is satisfied with an error of less than 1% in our calculation.

TABLE III. The dielectric properties for the three polytypes of BN: macroscopic dielectric constant ε_∞, static dielectric constant ε_0, and Born effective charge tensor Z^*.

ε_∞		ε_0		$\lvert Z^*\rvert$		
			c-BN			
4.54		6.74		1.89		present
4.5		7.1				exp.[a]
4.46		6.8				exp.[b]
3.86						calc.[c]
4.54				1.93		calc.[d]
$\varepsilon_\infty^{\perp c}$	$\varepsilon_\infty^{\parallel c}$	$\varepsilon_0^{\perp c}$	$\varepsilon_0^{\parallel c}$	$\lvert Z^{*\perp c}\rvert$	$\lvert Z^{*\parallel c}\rvert$	
			w-BN			
4.50	4.64	6.50	6.99	1.83	1.92	present
4.16	4.18					calc.[c]
4.50	4.67			1.86	1.96	calc.[d]
			h-BN			
4.85	2.84	6.61	3.38	2.71	0.82	present
4.95	4.1	6.85	5.06			exp.[e]
4.32	2.21					calc.[c]

[a]Reference 30.
[b]Reference 31.
[c]Reference 6.
[d]Reference 12.
[e]Reference 32.

TABLE IV. The TO and LO phonon frequencies (in cm^{-1}) at the Γ point of *c*-BN.

T_2(TO)	T_2(LO)	
1062	1295	present
1055.7	1304.8	exp.[a]
1056	1303	exp.[b]
1040	1285	calc.[c]

[a]Reference 31.
[b]Reference 33.
[c]Reference 12.

The average values of the macroscopic dielectric constant and the Born effective charge tensor are defined by $\overline{\varepsilon_\infty} = \frac{1}{3}\mathrm{Tr}\varepsilon_\infty$ and $\overline{Z^*} = \frac{1}{3}\mathrm{Tr}Z^*$, respectively, because their off-diagonal elements are equal to zero. For *w*-BN, the average values $\overline{\varepsilon_\infty} = 4.55$ and $\overline{Z^*} = 1.86$ are close to the values for *c*-BN. The degree of anisotropy of ε_∞ and Z^* can be estimated from the difference between the components parallel and perpendicular to the *c* axis: $\Delta\varepsilon_\infty = [\varepsilon_\infty^{\parallel c} - \varepsilon_\infty^{\perp c}]/\overline{\varepsilon_\infty}$ and $\Delta Z^* = [Z^{*\parallel c} - Z^{*\perp c}]/\overline{Z^*}$. The calculated anisotropies for *w*-BN are $\Delta\varepsilon_\infty = 0.03$ and $\Delta Z^* = 0.05$, and those for *h*-BN are $\Delta\varepsilon_\infty = 0.48$ and $\Delta Z^* = 0.91$. The anisotropy of *h*-BN is much larger than that of *w*-BN.

The calculated macroscopic dielectric constant along the *c* axis $\varepsilon_\infty^{\parallel c}$ and the static dielectric constant $\varepsilon_0^{\parallel c}$ for *h*-BN are 2.84 and 3.38, respectively. Xu and Ching[6] also reported a similar value, $\varepsilon_\infty^{\parallel c} = 2.21$. These values differ greatly from the experimental values $\varepsilon_\infty^{\parallel c} = 4.1$ and $\varepsilon_0^{\parallel c} = 5.06$ in Ref. 32. Although we repeated the calculation using the experimental lattice constants, the results $\varepsilon_\infty^{\parallel c} = 2.72$ and $\varepsilon_0^{\parallel c} = 3.17$ were not improved significantly. In connection with this discrepancy, more detailed investigation is desirable. For the other dielectric properties of the three BN polytypes, the agreement of the values obtained by the present calculation, experiment, and other computations is good.

C. Dynamical properties at the Γ point

The Γ-phonon frequencies for the three polytypes of BN were calculated by solving the eigenvalue problem of the dynamical matrix at the wave vector $\boldsymbol{q} = \boldsymbol{0}$. The calculated results for the Γ-phonon frequencies are shown in Tables IV, V, and VI. There is a triply degenerate optical phonon mode expressed with the symmetry T_2 at the Γ point of *c*-BN. This mode is active in both Raman and IR spectroscopy. The Γ-phonon modes of *w*-BN can be classified into the Raman

TABLE V. The TO and LO phonon frequencies (in cm^{-1}) at the Γ point of *w*-BN.

E_2	E_2	B_1	A_1(TO)	A_1(LO)	E_1(TO)	E_1(LO)	B_1	
475	979	982	1043	1280	1075	1293	1134	present
			1006	1258	1053	1281		calc.[a]

[a]Reference 12.

TABLE VI. The TO and LO phonon frequencies (in cm^{-1}) at the Γ point of *h*-BN.

E_{2g}	B_{1g}	A_{2u}(TO)	A_{2u}(LO)	B_{1g}	E_{2g}	E_{1u}(TO)	E_{1u}(LO)	
50	113	754	823	815	1382	1382	1614	present
52		783	828		1366	1367	1610	exp.[a]

[a]Reference 32 for A_{2u}(TO,LO) and E_{1u}(TO,LO) modes, and Ref. 34 for E_{2g} modes.

active and infrared active A_1 and E_1 modes, the two Raman active E_2 modes, and the two silent B_1 modes. For *h*-BN, there are the infrared active A_{2u} and E_{1u} modes, the two Raman active E_{2g} modes, and the two silent B_{1g} modes. Among these, each E_1, E_2, E_{1u}, and E_{2g} mode is doubly degenerate. The infrared active mode is divided into the transverse optical mode and the longitudinal optical (LO) mode, because BN is an ionic crystal and reflects the effect of Coulomb interactions (dipole-dipole interactions). We calculated the frequencies of the LO phonon mode by solving the eigenvalue problem for the dynamical matrix corresponding to the LO phonon mode as follows. Since the macroscopic dielectric constant and the Born effective charge tensor are related to the macroscopic electric field induced by the dipole-dipole interactions, the dynamical matrix for the LO phonon mode $D^{LO}_{I\alpha,J\beta}$ can be expressed as[11]

$$D^{LO}_{I\alpha,J\beta}=D^{TO}_{I\alpha,J\beta}+\frac{4\pi}{\Omega}\frac{\left(\sum_{\alpha'}\hat{q}_{\alpha'}Z^{*}_{I\alpha'\alpha}\right)\left(\sum_{\beta'}\hat{q}_{\beta'}Z^{*}_{J\beta'\beta}\right)}{\sqrt{M_I M_J}\sum_{\alpha\beta}\hat{q}_{\alpha}\varepsilon^{\infty}_{\alpha\beta}\hat{q}_{\beta}}, \tag{29}$$

where $D^{TO}_{I\alpha,J\beta}$ is the dynamical matrix for the TO phonon mode, which is directly obtained from the linear response calculation, $\varepsilon^{\infty}_{\alpha\beta}$ and $Z^{*}_{I\alpha'\alpha}$ are the elements of the macroscopic dielectric constant and the Born effective charge tensor, $\hat{q}_\alpha$ is the direction of the wave vector of the phonon, M_I is the atomic mass of the Ith atom, and $\{\alpha,\beta,\alpha',\beta'\}$ denotes the direction in a Cartesian coordinate system.

The calculated optical frequencies at the Γ point of the three BN polytypes agree very well with the experimental data from first-order Raman or IR spectroscopy in Refs. 31–34. The agreement of our results with other first-principles calculations for the Γ-phonon frequencies is reasonable, taking into account the variation of frequencies due to the differences of the computational methods and the equilibrium structural parameters.

The Γ-phonon frequencies of the T_2(TO,LO) mode of *c*-BN and the A_1(TO,LO) and E_1(TO,LO) modes of *w*-BN are close to each other. It is difficult to identify the crystal structure with these modes by Raman or IR spectroscopy. However, since the two Raman active E_2 modes exist only in *w*-BN, it is possible to distinguish *w*-BN from *c*-BN. On the other hand, it is easy to tell the crystal structure of *h*-BN from the others using Raman or IR spectroscopy, because the frequencies of the infrared or Raman active modes of *h*-BN differ from those of *c*-BN or *w*-BN.

IV. SUMMARY

We have performed a first-principles calculation on the structural, dielectric, and lattice-dynamical properties for the three polytypes of BN. In our calculation, the ultrasoft pseudopotential technique and density-functional perturbation theory are used. The calculated lattice constants and the experimental values are well in agreement except for *c* of *h*-BN. Each bulk modulus of *w*-BN and *c*-BN is close to the value for diamond, but *h*-BN is not so hard. From the calculated results of the cohesive energy, it is predicted that *c*-BN is the most stable structure at zero temperature. For the dielectric properties, the computed values are in reasonable agreement with experimental data except for the macroscopic dielectric constant along the *c* axis for *h*-BN. The average values of the macroscopic dielectric constant and the Born effective charge tensor of *w*-BN are close to those of *c*-BN. The calculated anisotropy for *h*-BN is much larger than that for *w*-BN. The phonon frequencies of the T_2(TO,LO) mode of *c*-BN and the A_1(TO,LO) and E_1(TO,LO) modes of *w*-BN are close to each other, but the two Raman active E_2 modes exist only in *w*-BN. Therefore, when crystal structural analysis is performed by the Raman spectroscopy, it is possible to distinguish *w*-BN from *c*-BN by investigating the two E_2 modes of *w*-BN. On the other hand, the frequencies of the infrared or Raman active modes of *h*-BN differ from those of *c*-BN and *w*-BN, and so it is easy to tell the crystal structure of *h*-BN from that of *c*-BN and *w*-BN by Raman spectroscopy or infrared reflectivity.

ACKNOWLEDGMENT

The authors thank Y. Hirose for giving them the opportunity to perform this study and also for helpful discussions.

[1] F.R. Corrigan and F.P. Bundy, J. Chem. Phys. **63**, 3812 (1975).
[2] S. Bohr, R. Haubner, and B. Lux, Diamond Relat. Mater. **4**, 714 (1995).
[3] H. Sachdev, R. Haubner, H. Nöth, and B. Lux, Diamond Relat. Mater. **6**, 286 (1997).
[4] V.L. Solozhenko, J. Hard Mater. **6**, 51 (1995).
[5] D. Vanderbilt, Phys. Rev. B **41**, 7892 (1990); K. Laasonen, A. Pasquarello, R. Car, C. Lee, and D. Vanderbilt, *ibid.* **47**, 10 142 (1993).
[6] Y.-N. Xu and W.Y. Ching, Phys. Rev. B **44**, 7787 (1991).

[7] G. Kern, G. Kresse, and J. Hafner, Phys. Rev. B **59**, 8551 (1999).
[8] K. Albe, Phys. Rev. B **55**, 6203 (1997).
[9] J. Furthmüller, J. Hafner, and G. Kresse, Phys. Rev. B **50**, 15 606 (1994).
[10] X. Gonze, Phys. Rev. B **55**, 10 337 (1997).
[11] X. Gonze and C. Lee, Phys. Rev. B **55**, 10 355 (1997).
[12] K. Karch and F. Bechstedt, Phys. Rev. B **56**, 7404 (1997).
[13] P. Hohenberg and W. Kohn, Phys. Rev. **136**, B864 (1964); W. Kohn and L.J. Sham, *ibid.* Phys. Rev. **140**, A1133 (1965).
[14] J.P. Perdew and Y. Wang, Phys. Rev. B **45**, 13 244 (1992).
[15] A.M. Rappe, K.M. Rabe, E. Kaxiras, and J.D. Joannopoulos, Phys. Rev. B **41**, 1227 (1990).
[16] H.J. Monkhorst and J.D. Pack, Phys. Rev. B **13**, 5188 (1976).
[17] A. Fukumoto and K. Miwa, Phys. Rev. B **55**, 11 155 (1996).
[18] D.D. Johnson, Phys. Rev. B **38**, 12 807 (1988).
[19] F.D. Murnaghan, Proc. Natl. Acad. Sci. USA **30**, 244 (1944).
[20] G.P. Francis and M.C. Payne, J. Phys.: Condens. Matter **2**, 4359 (1990).
[21] P. Pulay, Mol. Phys. **17**, 197 (1969).
[22] M. Bernasconi, G.L. Chiarotti, P. Focher, S. Scandolo, E. Tosatti, and M. Parrinello, J. Phys. Chem. Solids **56**, 501 (1995).
[23] A. Dal Corso, A. Pasquarello, and A. Baldereschi, Phys. Rev. B **56**, R11 369 (1997).
[24] S.G. Louie, S. Froyen, and M.L. Cohen, Phys. Rev. B **26**, 1738 (1982).
[25] R.H. Wentorf, Jr., J. Chem. Phys. **26**, 956 (1957).
[26] T. Soma, S. Sawaoka, and S. Saito, Mater. Res. Bull. **9**, 755 (1974).
[27] V.L. Solozhenko, G. Will, and F. Elf, Solid State Commun. **96**, 1 (1995).
[28] J.P. Perdew, K. Burke, and M. Ernzerhof, Phys. Rev. Lett. **77**, 3865 (1996); **78**, 1396(E) (1997).
[29] H.J. McSkimin and P. Andreatch, J. Appl. Phys. **43**, 985 (1972).
[30] P.J. Gielisse, S.S. Mitra, J.N. Plendl, R.D. Griffis, L.C. Mansur, R. Marshall, and E.A. Pascoe, Phys. Rev. **155**, 1039 (1967).
[31] M.I. Ecremets, M. Gauthier, A. Polian, J.C. Chervin, and J.M. Besson, Phys. Rev. B **52**, 8854 (1995).
[32] R. Geick, C.H. Perry, and G. Ruppercht, Phys. Rev. **146**, 543 (1966).
[33] O. Brafman, G. Lengyel, and S.S. Mitra, Solid State Commun. **6**, 523 (1968).
[34] T. Kuzuba, K. Era, T. Ishii, and T. Sato, Solid State Commun. **25**, 863 (1978).